Measurements of Higgs boson production through vector boson fusion in the $H \to WW^* \to e\nu\mu\nu$ final state at $\sqrt{s}$ = 13 TeV with the ATLAS detector

ICPPA 2022 Conference (Moscow, Russia, 29.11-2.12.2022)

Ekaterina Ramakoti
(on behalf of ATLAS Collaboration)
NRC Kurchatov Institute

arXiv:2207.00338
(all plots and tables are taken from this reference unless stated otherwise)

$H \to WW^* \to e\nu\mu\nu$

The Higgs boson decay channel:

$$H \to WW^* \to e\nu\mu\nu$$

21.6% 0.5%

m_H = 125.09 GeV

VBF is the only process considered as signal in the analysis.

Background processes (slide 12):

- others H-boson
- top quark production (*tW* and $t\bar{t}$)
- non-resonant *WW*
- dibosons (WZ, ZZ, Wγ, Wγ* and Zγ)
- Drell-Yan (*Z+jets* or $Z/\gamma^* \to \tau\tau$)
- Mis-Id (*W+jets*) and multi-jets (QCD)
  jets misidentified as ℓ

- clear signature
- two isolated leptons
- sizeable missing E_T
- only m_T reconstruction
- two highly energetic forward jets

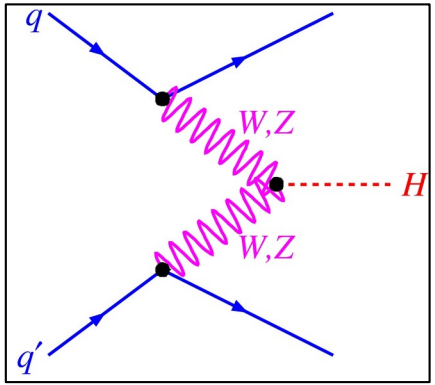

Vector boson fusion (vbf)

source

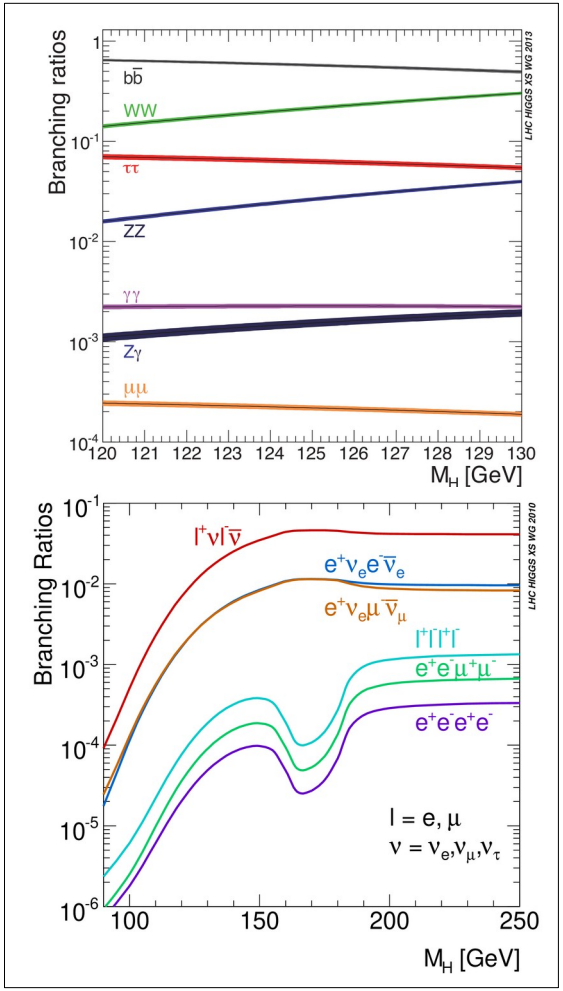

Event selection

Signal Region

Category	$N_{\text{jet},(p_T>30\text{ GeV})} \geq 2$ VBF
Preselection	Two isolated, different-flavor leptons ($\ell = e, \mu$) with opposite charge $p_T^{\text{lead}} > 22$ GeV , $p_T^{\text{sublead}} > 15$ GeV $m_{\ell\ell} > 10$ GeV
Background rejection	$N_{b\text{-jet},(p_T>20\text{ GeV})} = 0$ $m_{\tau\tau} < m_Z - 25$ GeV
$H \to WW^* \to e\nu\mu\nu$ topology	central jet veto outside lepton veto $m_{jj} > 120$ GeV
Discriminating fit variable	DNN

Control Region

CR	$N_{\text{jet},(p_T>30\text{ GeV})} \geq 2$ VBF
$t\bar{t}/Wt$	$N_{b\text{-jet},(p_T>20\text{ GeV})} = 1$ $m_{\tau\tau} < m_Z - 25$ GeV central jet veto outside lepton veto
Z/γ^*	$N_{b\text{-jet},(p_T>20\text{ GeV})} = 0$ $m_{\ell\ell} < 70$ GeV $\lvert m_{\tau\tau} - m_Z \rvert \leq 25$ GeV central jet veto outside lepton veto

DNN (Deep Neural Network) is applied in the SR that uses 15 dicriminant variables: $\Delta\varphi_{\ell\ell}$, $m_{\ell\ell}$, m_T, Δy_{jj}, m_{jj}, p_T^{tot}, $\Sigma_\ell C_\ell$, $m_{\ell 1j1}$, $m_{\ell 1j2}$, $m_{\ell 2j1}$, $m_{\ell 2j2}$, p_T^{jet1}, p_T^{jet2}, p_T^{jet3} and E_T^{miss} significance

Distributions of m_{jj} and Δy_{jj} in the SR

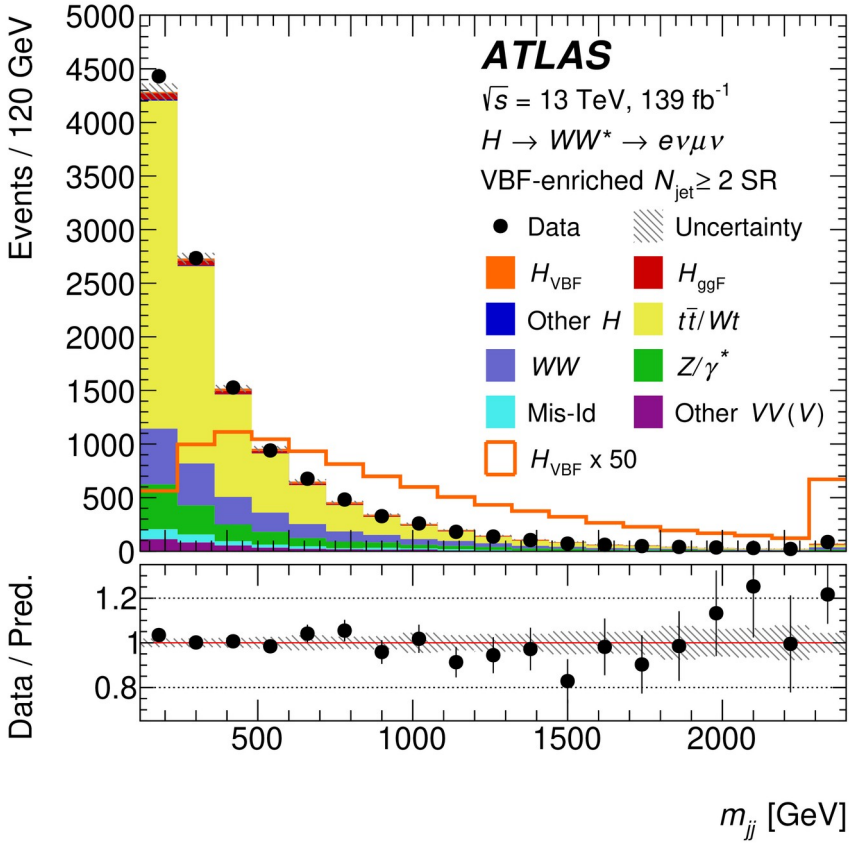

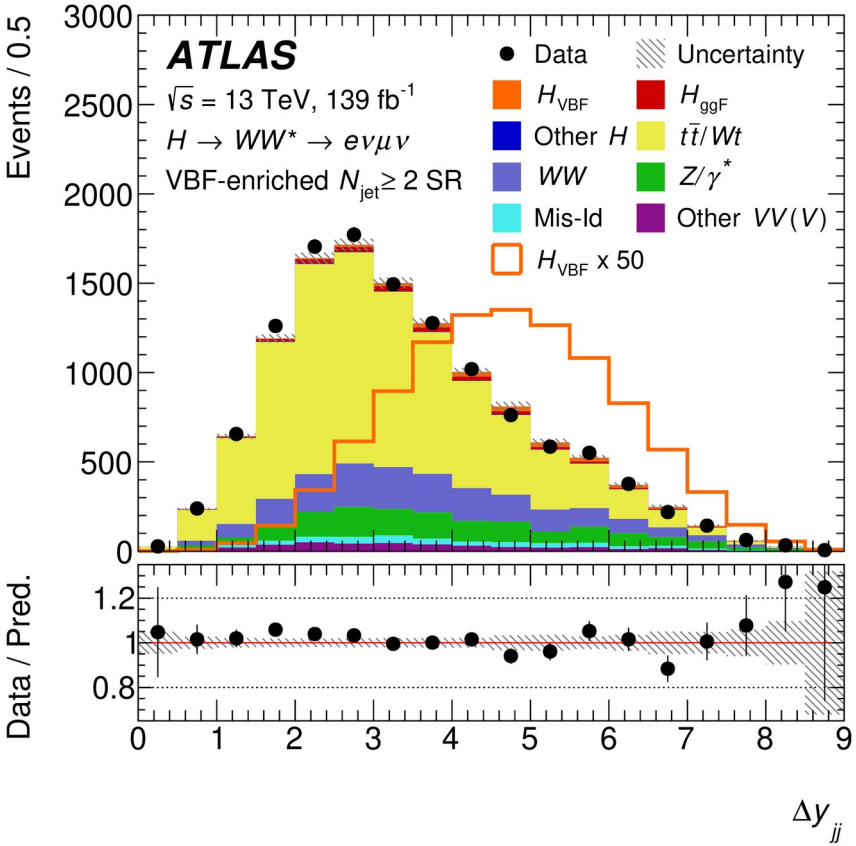

m_{jj} and Δy_{jj} provide best discrimination between signal and background

CRs for the most interesting bkgs

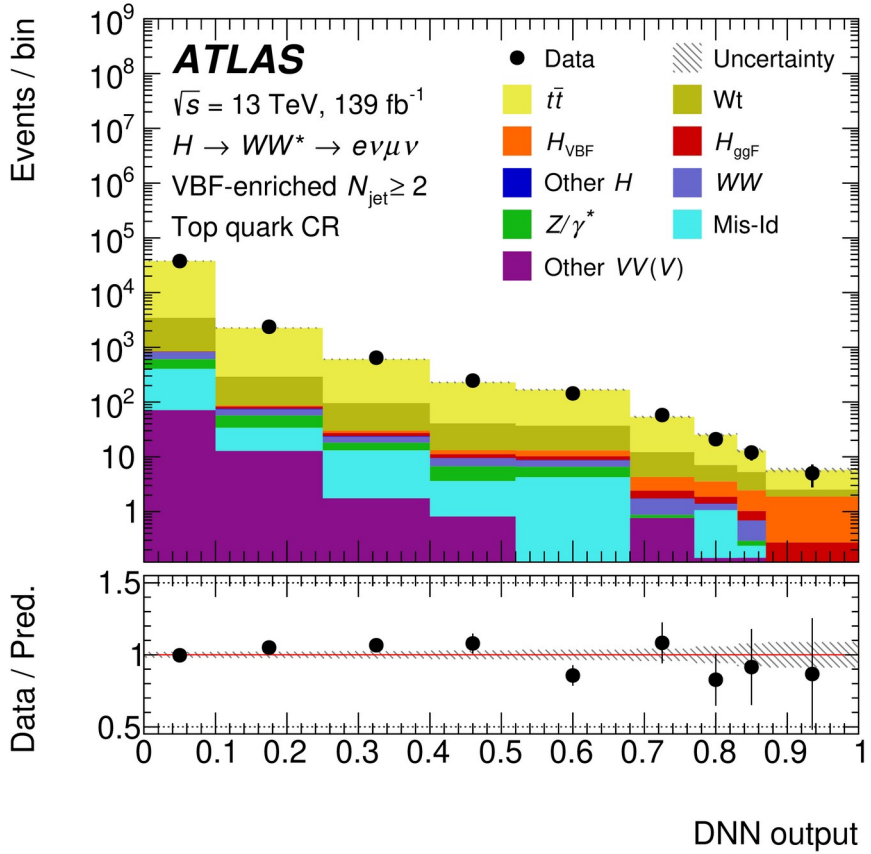

The post-fit NFs

$t\bar{t}/Wt$	Z/γ^*
$0.92^{+0.33}_{-0.21}$	$0.93^{+0.23}_{-0.19}$

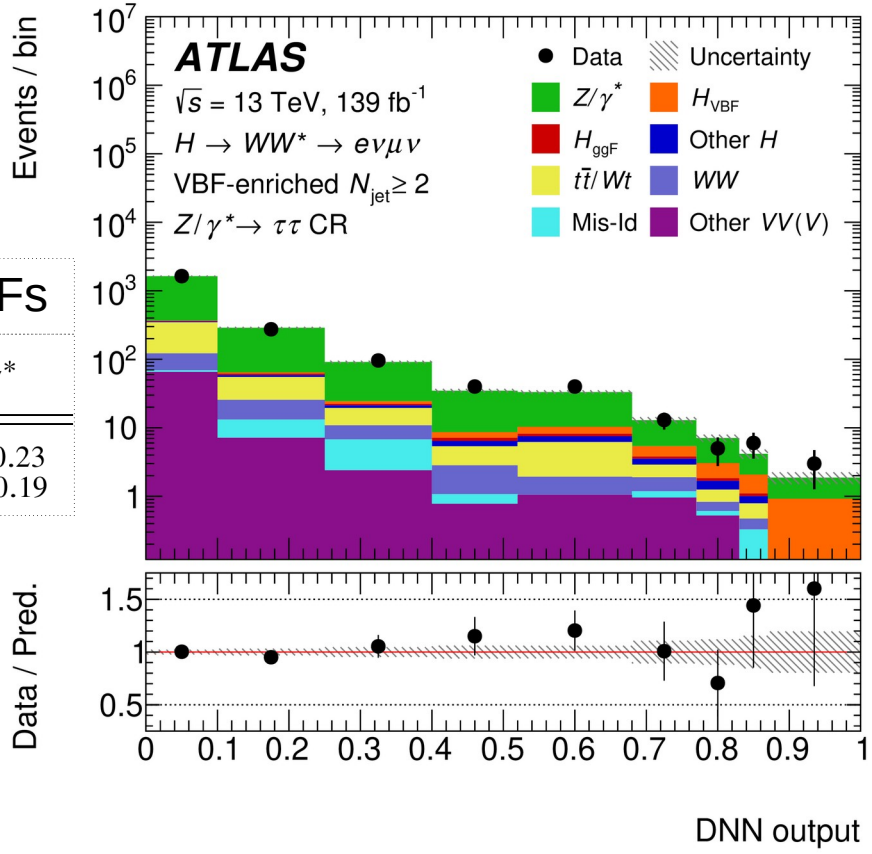

WW CR has no high purity due to the overwhelming background from top quark processes.

Post-fit yields and distribution in SRs

Process	$N_{\text{jet}} \geq 2$ VBF Inclusive	$N_{\text{jet}} \geq 2$ VBF DNN: [0.87, 1.0]
H_{ggF}	209 ± 40	2.6 ± 0.9
H_{VBF}	180 ± 40	28.8 ± 5.5
Other Higgs	29 ± 15	0.04 ± 0.02
WW	2100 ± 340	4.6 ± 1.2
$t\bar{t}/Wt$	7600 ± 370	2.6 ± 0.8
Z/γ^*	1300 ± 300	0.6 ± 0.1
Other VV	380 ± 80	0.6 ± 0.1
Mis-Id	330 ± 40	1.7 ± 0.2
Total	$12\,200 \pm 180$	42.0 ± 5.1
Observed	12 189	38

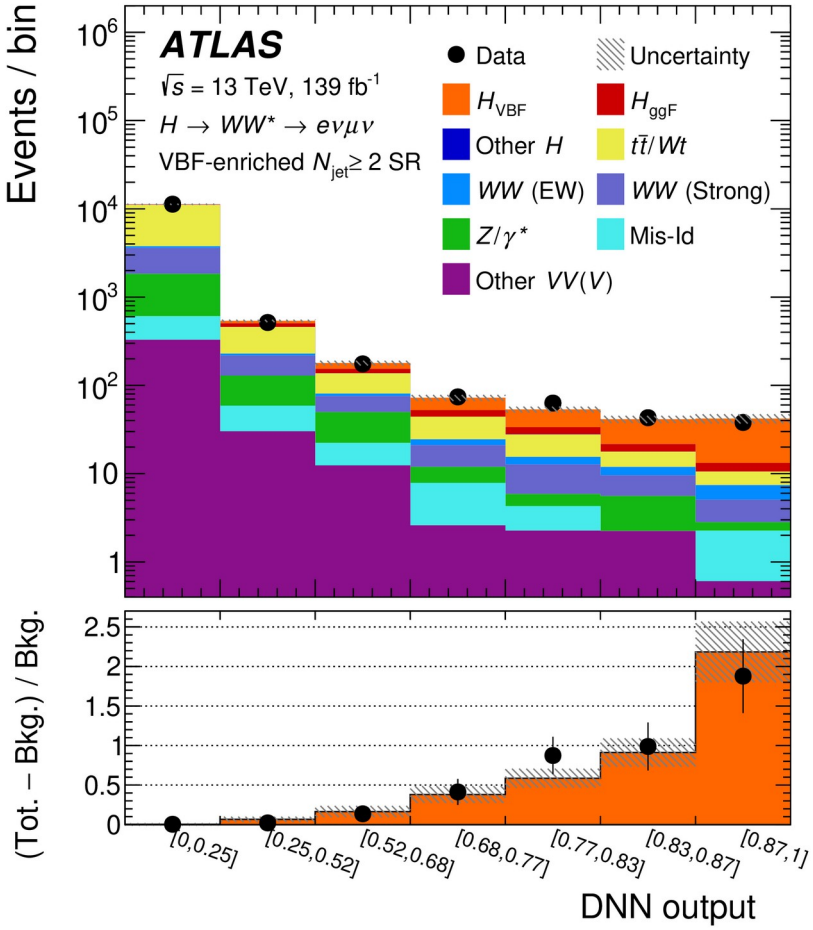

$Z_{\text{obs}} = 5.8\sigma$
$Z_{\text{exp}} = 6.2\sigma$

(Reduced) STXS categorization

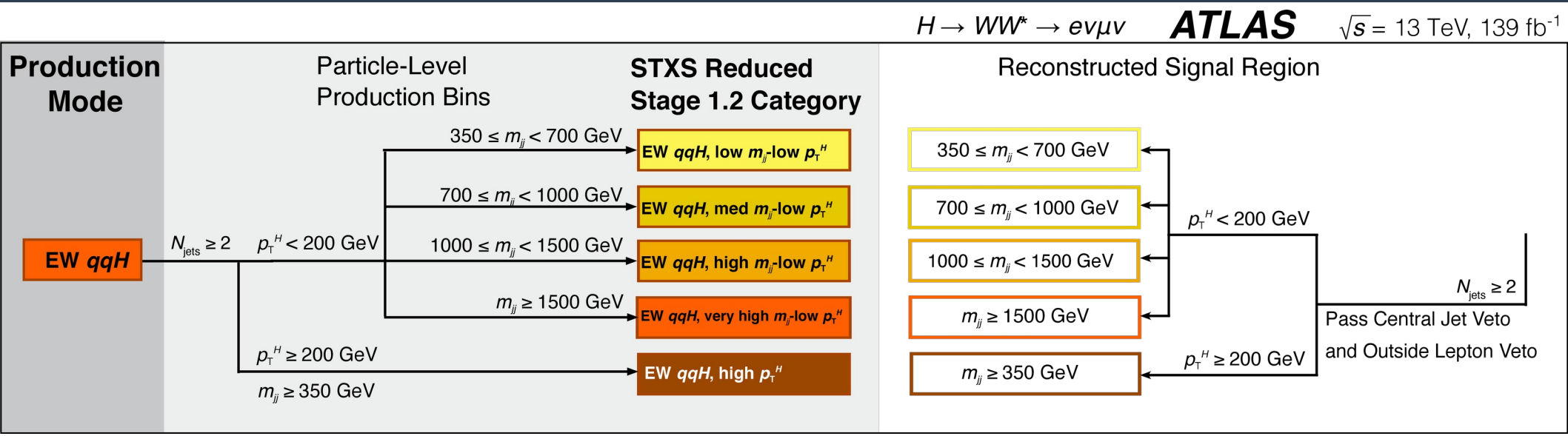

Each SR and corresponding CR are further divided which provides independent XS measurements in different sub-regions

STXS - simplified template cross sections

p_T^H is defined at the reconstruction level as the transverse momentum of Higgs boson candidate

Measured VBF cross-sections, total and STXS

Slide 14

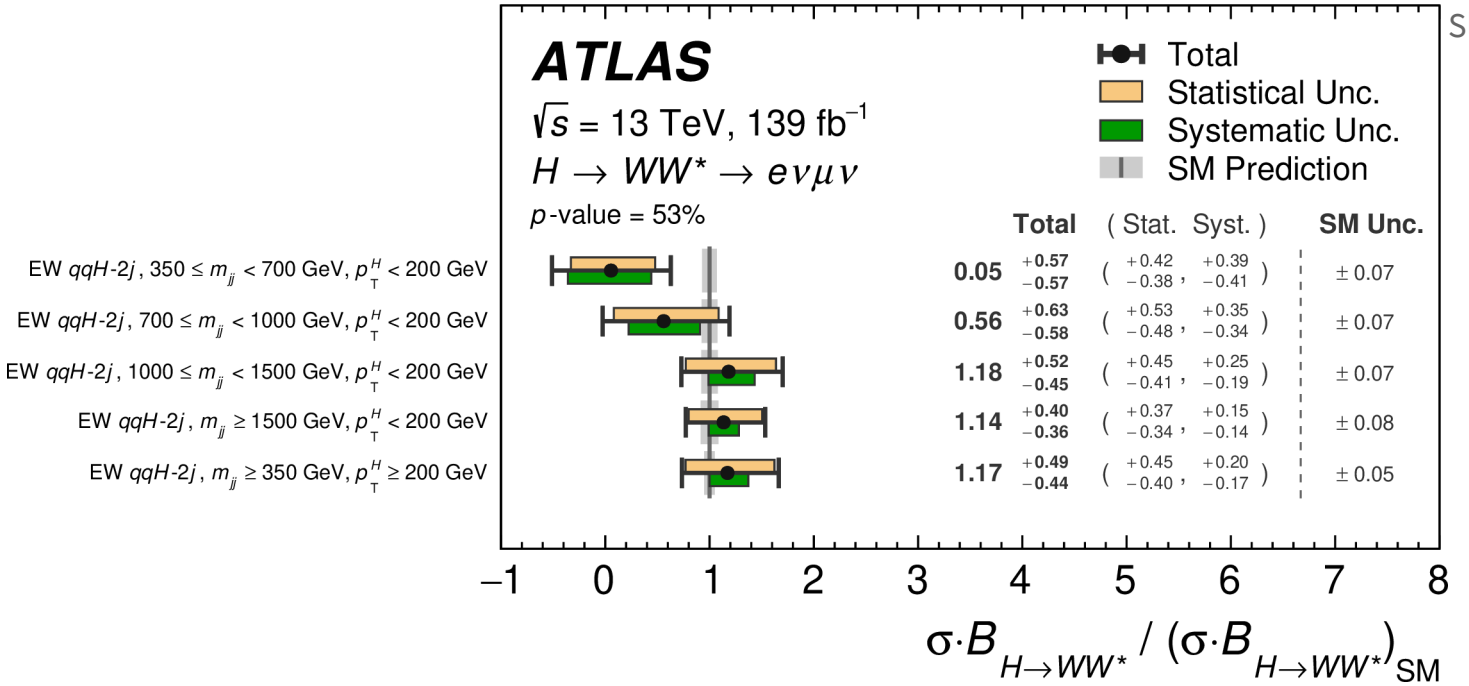

$$\sigma_{\mathrm{VBF}} \cdot \mathcal{B}_{H\to WW^*} = 0.75\,^{+0.19}_{-0.16}\ \mathrm{pb}$$

$$= 0.75 \pm 0.11\ (\mathrm{stat.})\ ^{+0.07}_{-0.06}\ (\mathrm{exp.\ syst.})\ ^{+0.12}_{-0.08}\ (\mathrm{sig.\ theo.})\ ^{+0.07}_{-0.06}\ (\mathrm{bkg.\ theo.})\ \mathrm{pb}$$

compared to the SM predicted value of 0.81 ± 0.02 pb

Breakdown of the main contributions to the total uncertainty

Source	$\frac{\Delta\sigma_{\mathrm{VBF}}\cdot\mathcal{B}_{H\to WW^*}}{\sigma_{\mathrm{VBF}}\cdot\mathcal{B}_{H\to WW^*}}$ [%]
Data statistical uncertainties	15
Total systematic uncertainties	18
MC statistical uncertainties	4.9
Experimental uncertainties	6.7
Flavor tagging	1.0
Jet energy scale	3.7
Jet energy resolution	2.1
$E_{\mathrm{T}}^{\mathrm{miss}}$	4.9
Muons	0.8
Electrons	0.4
Fake factors	0.8
Pileup	1.3
Luminosity	2.2

Source	$\frac{\Delta\sigma_{\mathrm{VBF}}\cdot\mathcal{B}_{H\to WW^*}}{\sigma_{\mathrm{VBF}}\cdot\mathcal{B}_{H\to WW^*}}$ [%]
Theoretical uncertainties	16
ggF	4.6
VBF	12
WW	5.5
Top	6.4
$Z\tau\tau$	1.0
Other VV	1.5
Other Higgs	0.4
Background normalizations	4.9
WW	0.6
Top	3.4
$Z\tau\tau$	3.4
Total	23

ATLAS and CMS results for VBF H→WW *

- CMS 25 fb^{-1} (7+8 TeV), link
  JHEP01 (2014) 096

$$\mu_{VBF} = 0.62^{+0.58}_{-0.47}$$

- ATLAS 25 fb^{-1} (7+8 TeV), link
  Phys. Rev. D 92, 012006 (2015)

$$\mu_{VBF} = 1.27^{+0.53}_{-0.45}$$

- ATLAS 36 fb^{-1}, link
  Phys. Lett. B 789 (2019) 508

$$\mu_{VBF} = 0.62^{+0.36}_{-0.35}$$

- CMS 138 fb^{-1}, link
  JHEP03(2021)003

$$\mu_{VBF} = 0.71^{+0.28}_{-0.25}$$

- ATLAS 139 fb^{-1}, link
  arXiv:2207.00338v1 (2022)

$$\mu_{VBF} = 0.93^{+0.23}_{-0.20}$$

Signal strength is measured with ~25% precision in ATLAS

backup

Others main background processes

ggH

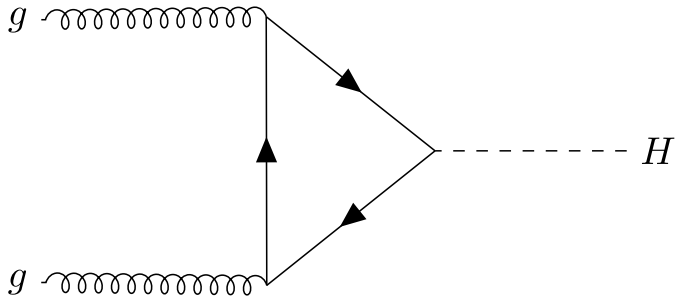

VH

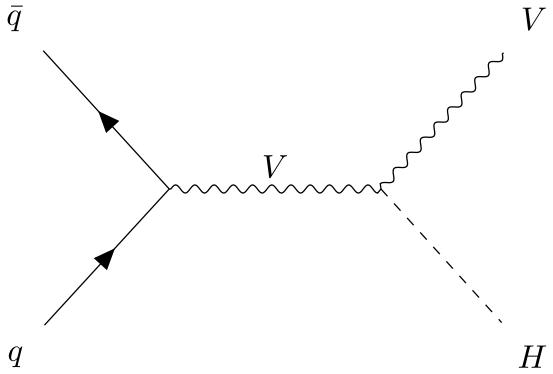

ttH

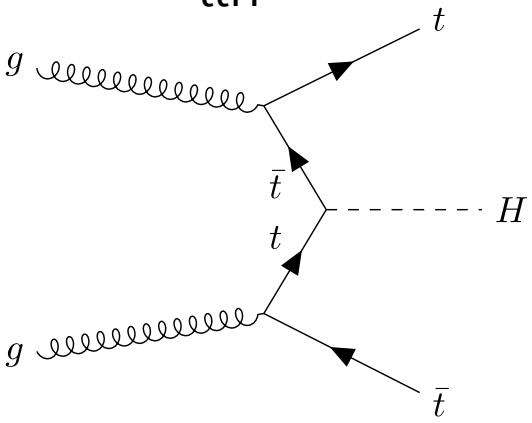

WW

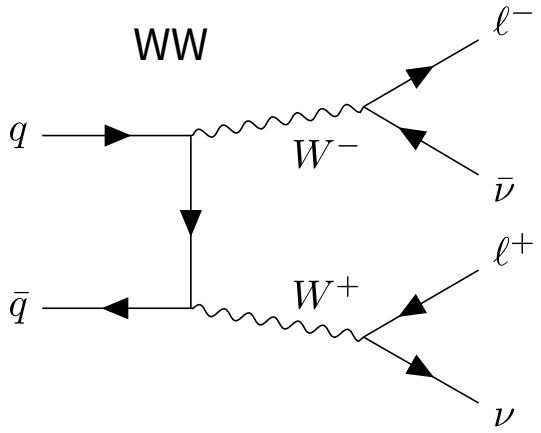

top

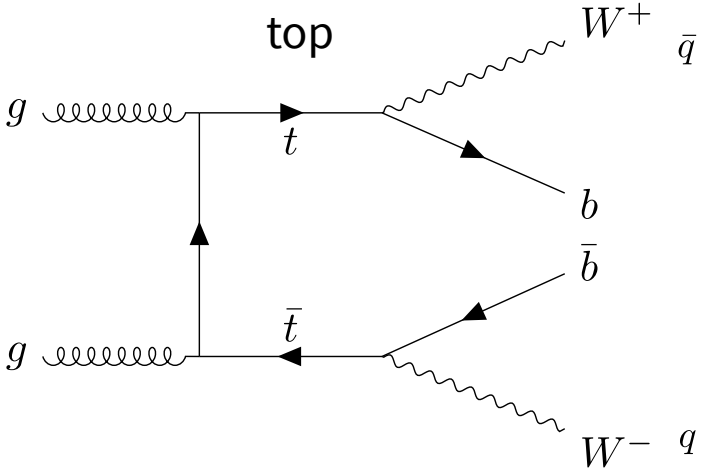

DY

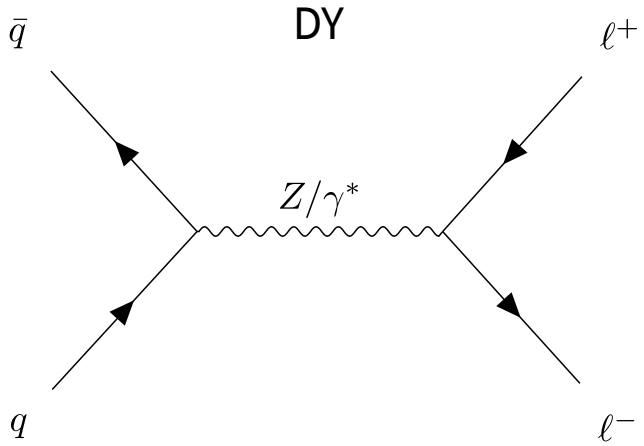

Overview of simulation tools used to generate processes

Process	Matrix element (alternative)	PDF set	UEPS model (alternative model)	Prediction order for total cross section
ggF H	POWHEG BOX v2 [23–27] NNLOPS [26, 30, 43] (MG5_aMC@NLO) [49, 86]	PDF4LHC15NNLO [57]	PYTHIA 8 [28] (HERWIG 7) [48]	N^3LO QCD + NLO EW [11, 33–42]
VBF H	POWHEG BOX v2 [23–25, 43] (MG5_aMC@NLO)	PDF4LHC15NLO	PYTHIA 8 (HERWIG 7)	NNLO QCD + NLO EW [44–46]
VH excl. $gg \to ZH$	POWHEG BOX v2	PDF4LHC15NLO	PYTHIA 8	NNLO QCD + NLO EW [52–56]
$t\bar{t}H$	POWHEG BOX v2	NNPDF3.0NLO	PYTHIA 8	NLO [11]
$gg \to ZH$	POWHEG BOX v2	PDF4LHC15NLO	PYTHIA 8	NNLO QCD + NLO EW [90, 91]
$qq \to WW$	SHERPA 2.2.2 [69] (Q_{cut})	NNPDF3.0NNLO [50]	SHERPA 2.2.2 [70, 71, 73–76] (SHERPA 2.2.2 [71, 72]; μ_{q})	NLO [77, 78, 92]
$qq \to WWqq$	MG5_aMC@NLO [49]	NNPDF3.0NLO	PYTHIA 8 (HERWIG 7)	LO
$gg \to WW/ZZ$	SHERPA 2.2.2	NNPDF3.0NNLO	SHERPA 2.2.2	NLO [93]
$WZ/V\gamma^*/ZZ$	SHERPA 2.2.2	NNPDF3.0NNLO	SHERPA 2.2.2	NLO [94]
$V\gamma$	SHERPA 2.2.8 [69]	NNPDF3.0NNLO	SHERPA 2.2.8	NLO [94]
VVV	SHERPA 2.2.2	NNPDF3.0NNLO	SHERPA 2.2.2	NLO
$t\bar{t}$	POWHEG BOX v2 (MG5_aMC@NLO)	NNPDF3.0NLO	PYTHIA 8 (HERWIG 7)	NNLO+NNLL [95–101]
Wt	POWHEG BOX v2 (MG5_aMC@NLO)	NNPDF3.0NLO	PYTHIA 8 (HERWIG 7)	NNLO [102, 103]
Z/γ^*	SHERPA 2.2.1 (MG5_aMC@NLO)	NNPDF3.0NNLO	SHERPA 2.2.1	NNLO [79]

Best-fit values and uncertainties for $\sigma_i \cdot B_{H \to WW^*}$

STXS bin ($\sigma_i \cdot \mathcal{B}_{H \to WW^*}$)	Value [fb]	Uncertainty [fb] Total	Stat.	Exp. Syst.	Sig. Theo.	Bkg. Theo.	SM prediction [fb]
EW qqH-2j, low m_{jj}-low p_T^H $350 \le m_{jj} < 700$ GeV, $p_T^H < 200$ GeV	6	$^{+63}_{-62}$	$^{+46}_{-42}$	$^{+31}_{-34}$	$^{+11}_{-14}$	$^{+24}_{-26}$	109 ± 7
EW qqH-2j, med m_{jj}-low p_T^H $700 \le m_{jj} < 1000$ GeV, $p_T^H < 200$ GeV	31	$^{+35}_{-33}$	$^{+30}_{-27}$	$^{+15}_{-14}$	$^{+8}_{-7}$	$^{+11}_{-10}$	56 ± 4
EW qqH-2j, high m_{jj}-low p_T^H $1000 \le m_{jj} < 1500$ GeV, $p_T^H < 200$ GeV	60	$^{+26}_{-23}$	$^{+23}_{-21}$	$^{+7}_{-7}$	$^{+9}_{-5}$	$^{+5}_{-5}$	51 ± 4
EW qqH-2j, very high m_{jj}-low p_T^H $m_{jj} \ge 1500$ GeV, $p_T^H < 200$ GeV	57	$^{+20}_{-18}$	$^{+18}_{-17}$	$^{+5}_{-5}$	$^{+3}_{-3}$	$^{+4}_{-4}$	50 ± 4
EW qqH-2j, high p_T^H $m_{jj} \ge 350$ GeV, $p_T^H \ge 200$ GeV	37	$^{+16}_{-14}$	$^{+14}_{-13}$	$^{+4}_{-3}$	$^{+4}_{-3}$	$^{+3}_{-3}$	32 ± 1

5 STXS bins for VBF

Correlations between the cross-section measurements

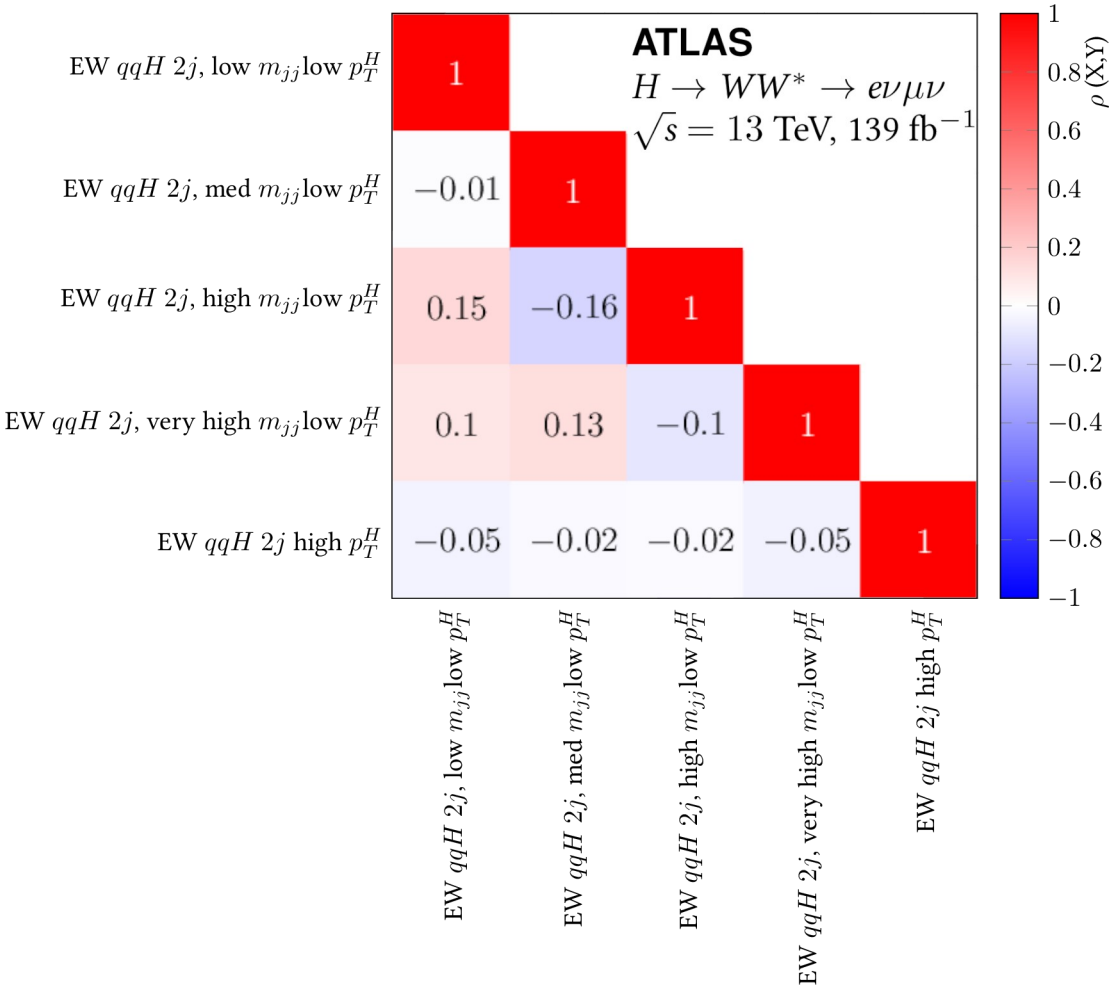

5 STXS bins for VBF

STXS Composition

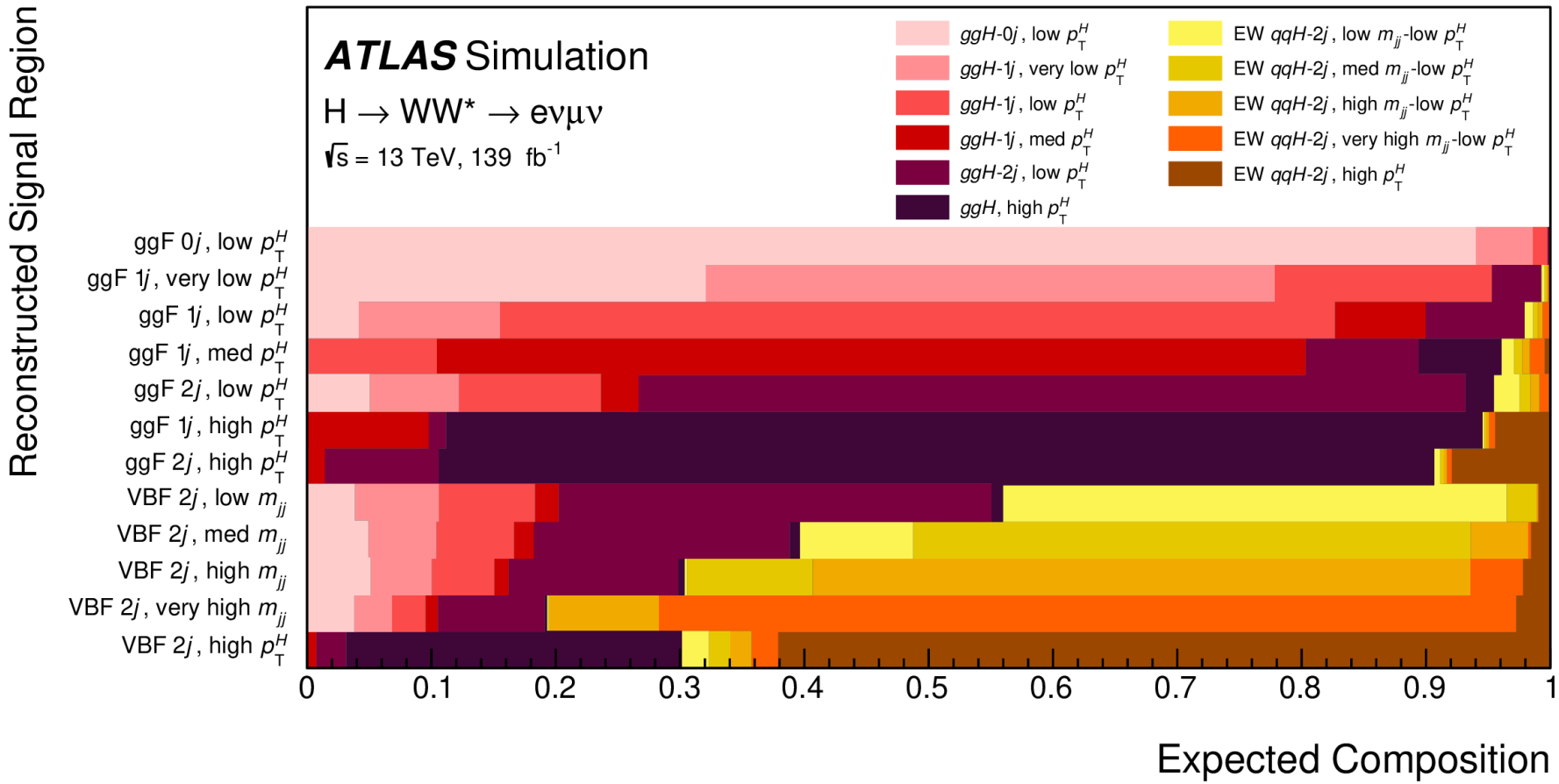

MT2 definition

$$m_{\mathrm{T2}}^2 = \min_{\not{p}_1+\not{p}_2=\not{p}_{\mathrm{T}}} \left[\max\{m_{\mathrm{T}}^2(p_{\mathrm{T}}^a, \not{p}_1), m_{\mathrm{T}}^2(p_{\mathrm{T}}^b, \not{p}_2)\}\right]$$

where the minimization is over all possible two-momenta, $\overline{p}_{1,2}$, such that their sum gives the observed missing transverse momentum $\overline{p}_T$, and where each of p_T^a and p_T^b is the combined transverse momentum of a charged lepton and a jet.

- $m^2_{T2} \leq m^2_W$ (decay of a pair of W each with a single invisible particle)
- $m^2_T \leq m^2_W$ (decay with single invisible particle)

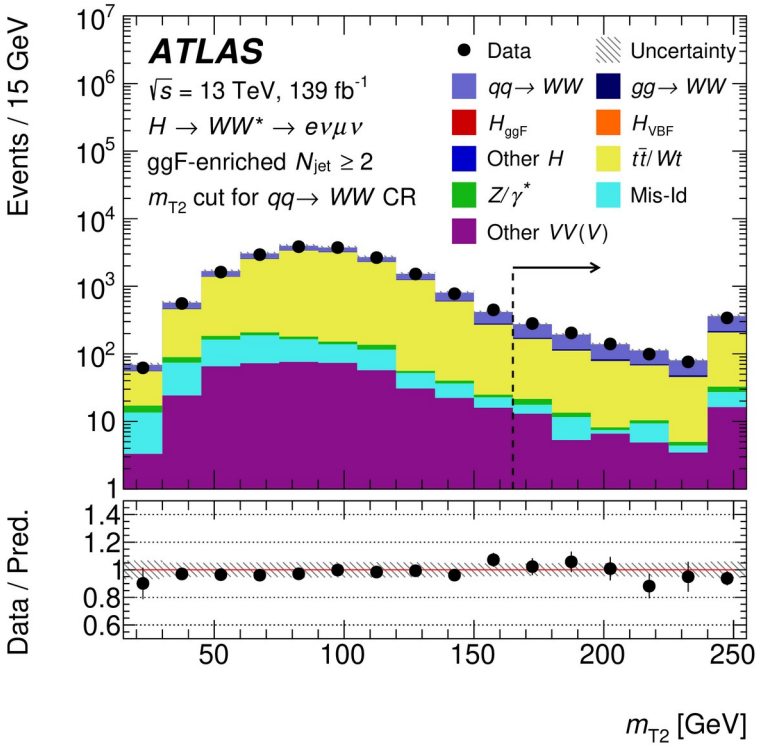

Post-fit yields for ggf in SRs

Process	$N_{jet} = 0$ ggF	$N_{jet} = 1$ ggF	$N_{jet} \geq 2$ ggF
H_{ggF}	2100 ± 220	1100 ± 130	440 ± 90
H_{VBF}	23 ± 9	103 ± 30	46 ± 12
Other Higgs	40 ± 20	55 ± 28	55 ± 27
WW	9700 ± 350	3500 ± 410	1500 ± 470
$t\bar{t}/Wt$	2200 ± 210	5300 ± 340	6100 ± 500
Z/γ^*	140 ± 50	280 ± 40	930 ± 70
Other VV	1400 ± 130	840 ± 100	470 ± 90
Mis-Id	1200 ± 130	720 ± 90	470 ± 50
Total	$16\,770 \pm 130$	$11\,940 \pm 110$	$10\,030 \pm 100$
Observed	16 726	11 917	9 982

Measured ggF cross-sections, total and STXS

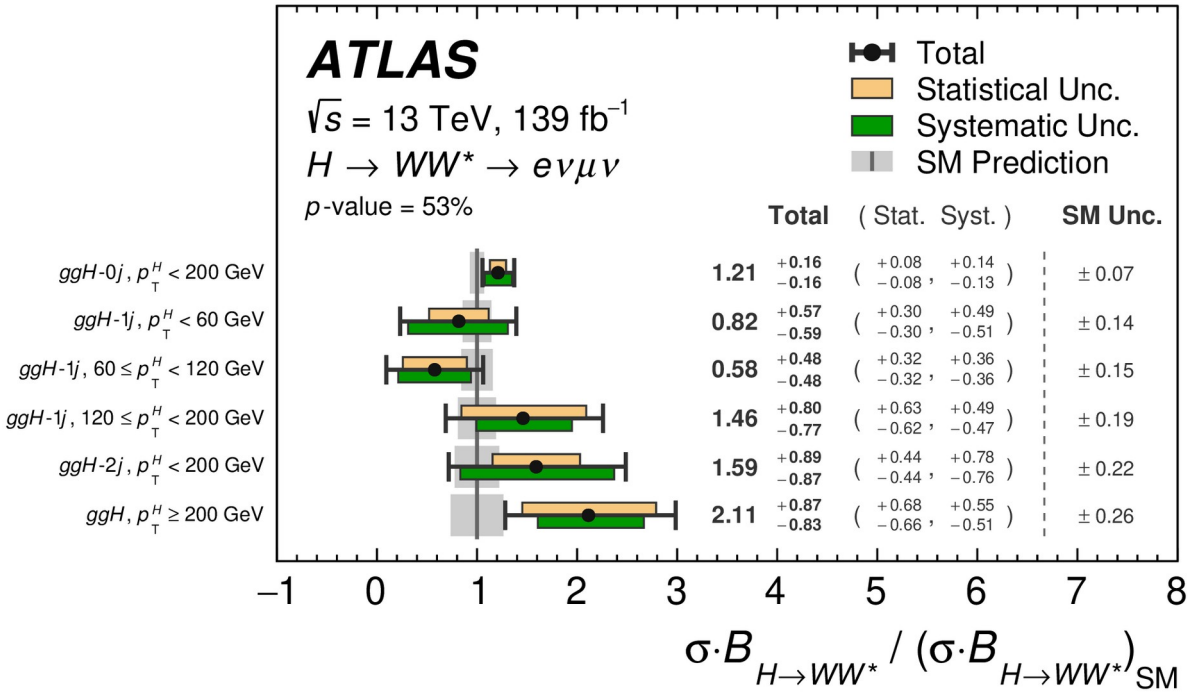

$$\sigma_{\mathrm{ggF}} \cdot \mathcal{B}_{H\to WW^*} = 12.0 \pm 1.4 \text{ pb}$$

$$= 12.0 \pm 0.6 \text{ (stat.)}^{+0.9}_{-0.8} \text{ (exp. syst.)}^{+0.6}_{-0.5} \text{ (sig. theo.)} \pm 0.8 \text{ (bkg. theo.) pb}$$

compared to the SM predicted values of 10.4 ± 0.5 pb

ATLAS and CMS results for ggF H→WW*

- **ATLAS Run1** PRD 92 (2015) 012006 $\mu_{ggF} = 1.02^{+0.29}_{-0.26}$
- **ATLAS Run2 36 fb^{-1}** Phys. Lett. B 789 (2019) 508 $\mu_{ggF} = 1.10^{+0.21}_{-0.20}$
- **ATLAS Run2 139 fb^{-1}** Current $\mu_{ggF} = 1.15^{+0.14}_{-0.13}$
  Factor of 1.5 improvement
- **CMS Run1** JHEP01 (2014) 096 $\mu_{ggF} = 0.76 \pm 0.21$
- **CMS 138 fb^{-1}** arXiv:2206.09466 $\mu_{ggF} = 0.92^{+0.11}_{-0.10}$
  same-flavour channel included
- Signal strength is measured with ~12% precision in both experiments